Published in final edited form as:
J Struct Biol. 2009 May ; 166(2): 172–182. doi:10.1016/j.jsb.2009.02.005.

Structure-function relationships of the outer membrane translocon Wza investigated by cryo-electron microscopy and mutagenesis

Robert C. Ford[1,*], **Anne L. Brunkan-LaMontagne**[2,*], **Richard F. Collins**[3], **Bradley R. Clarke**[2], **Robert Harris**[2], **James H. Naismith**[4], and **Chris Whitfield**[2]

[1]Department of Molecular and Cellular Biology, The University of Guelph, Guelph, Ontario, N1G 2W1, Canada.

[2]Manchester Interdisciplinary Biocentre, Faculty of Life Sciences, University of Manchester, M1 7DN, UK.

[3]Manchester Interdisciplinary Biocentre, Faculty of Engineering and Physical Sciences, University of Manchester, M1 7DN, UK.

[4]Centre for Biomolecular Sciences, The University of St Andrews, Fife KY16 9RH, UK.

Summary

The outer membrane protein, Wza from *E. coli* K30, forms an octameric complex that is essential for capsular polysaccharide export. Homologs of Wza are widespread in gram-negative bacterial pathogens where capsules are critical virulence determinants. Wza is unusual in that it spans the outer membrane using a barrel composed of amphipathic α-helices, rather than being a β-barrel like almost all other outer membrane channels. The transmembrane helical barrel of Wza also forms the external opening to a hydrophilic translocation pathway that spans the periplasm. Here, we have probed the structure and function of the Wza complex using both cryo-electron microscopy and mutagenesis. The helical barrel structure is stable in detergent micelles under mildly acidic conditions but is destabilised at basic pH, although the overall quaternary structure is retained. Truncation of the C-terminal region that forms the helical barrel by 4 residues has no effect on the ability of Wza to oligomerize and support capsule export, but larger truncations of 18, 24 or 35 amino acids abolish its function. The bulk of the C-terminal domain is essential for the stability and assembly of the *E. coli* Wza complex.

Keywords

Outer membrane protein; capsular polysaccharide; transport; Wza; cryo-electron microscopy

Introduction

The biosynthesis and export of polysaccharides that constitute the extracellular protective capsules of gram-negative bacteria [1, 2] is a process that requires the presence of many proteins with components in the cytoplasm, periplasm, and the inner and outer membranes [3]. An essential component of this machinery is the outer membrane protein Wza. Wza

Co-corresponding authors: R.C. Ford, Manchester Interdisciplinary Biocentre, Faculty of Life Sciences, University of Manchester, M1 7DN, UK. bob.ford@manchester.ac.uk and C. Whitfield, Department of Molecular and Cellular Biology, The University of Guelph, Guelph, Ontario, N1G 2W1, Canada. cwhitfie@uoguelph.ca.
*These authors contributed equally to the work.

Europe PMC Funders Author Manuscripts

forms an octameric complex thought to provide the translocation pathway across the outer membrane [4, 5]. Wza is proposed to interact with other components of the process, notably with a tetramer of Wzc, an inner membrane protein, as well as with the polysaccharide [6-10]. Structural data for much of the machinery involved in polysaccharide export is limited, but a high resolution crystal structure is available for the Wza octamer [5]. In the Wza complex, each monomer is composed of four domains arranged parallel to the 8-fold symmetry axis, such that four distinct rings of domains are formed (termed rings R1-R4, see Fig. 2). At the centre of each ring is a water-filled space so that the complex encloses a long hydrophilic cavity running along the C8 symmetry axis. Domains composing rings R1-R3 are all typical of small water-soluble domains, with a mix of helical and β sheet structure, hydrophobic cores and hydrophilic external faces. However, domains in ring R4 are atypical, and are composed of a single long α-helix at the C-terminus of each protein and a short N-terminal region that wraps around the bottom of ring R4 like a collar. Each long α-helix in ring R4 is amphipathic, which allows the octameric barrel of helices to display a hydrophobic exterior-facing surface and a hydrophilic interior. The helices do not run parallel to the C8 symmetry axis, but are slanted at an angle of about 45° to it, and also curved so that there is a twist to the barrel. At each end, the helical barrel is open, with a ~17Å diameter opening to the external medium at one end, and a slightly wider opening into the central cavity of the complex at the other. A constriction of the barrel occurs at the centre (~14Å diameter), where a ring of charged residues (His365, Asp366 and Glu369) protrudes into the interior.

Although the long hydrophilic cavity in Wza is open at the top, it is closed at the bottom by the domains forming ring R1. It seems essential that either the R1 domain undergoes a conformational change to create an opening at the base, or alternatively R2 and R3 adjust their relative positions to create a side portal for polysaccharide to move into and through the complex [3, 5]. The R1 domain and possibly the R2 domain interact with a periplasmic domain of the Wzc tetramer [9-11]. Wzc is an inner membrane protein whose function in capsule assembly is dictated by a cytoplasmic C-terminal domain containing multiple tyrosine residues that can be phosphorylated. Wzc has endogenous tyrosine autokinase activity[6] and phosphorylation load seems important because its cognate phosphatase (Wzb) is also essential for capsule assembly [7, 12] . The essential components of this system are conserved in a range of gram negative bacteria, including important pathogens of plants and animals, as well as bacteria that produce polymers of commercial value[3].

Several lines of evidence support the hypothesis that ring R4 is the transmembrane region of Wza: (i) In the crystal structure, no other region on the outer surface of the complex displays a region devoid of charged side chains and depleted in hydrophilic side chains [5]. (ii) Density for a few detergent molecules or lipid anchors can be found in the X-ray crystallography-derived density map surrounding the helical barrel [5]. (iii) A Flag-tag epitope engineered at the C-terminus of Wza is found to be exposed to the extracellular medium [5]. (iii) Electron microscopy of Wza reconstituted into lipid bilayers shows that the complex inserts asymmetrically into the membrane, with three bands of density of total dimensions ~90Å emerging on one side of the membrane into the negative stain [10].

The structural database of membrane proteins is rather small [13], but one common feature that emerges from a cursory examination is that whilst bacterial inner membrane proteins tend to span the membrane using α-helical elements, bacterial outer membrane proteins (with one exception, Wza) span the membrane using β strands organised into a β barrel [14-17]. Eukaryotic membrane proteins, about which even less is known, appear to resemble the inner membrane proteins of bacteria, with α-helical transmembrane spanning regions. Given that Wza represents an exception (an outer membrane protein with α-helical transmembrane spanning regions), it is appropriate that a closer examination of the factors

influencing the assembly and stability of the protein be carried out, especially for the structurally unique region, R4. Proteins sharing sequence motifs with Wza are widespread in the bacterial databases, many being involved in bacterial polysaccharide assembly. However, the Wza structural organisation could be representative of another class of important outer membrane proteins called secretins. These proteins are involved in the export of proteins across the outer membrane and the databases identify many hundreds of known examples [17]. Although there are no high resolution structures for secretins, lower resolution electron microscopy studies suggest that representative proteins such as PilQ [18, 19] and PulD [20, 21] which do not share any sequence similarity with Wza, nevertheless may share a similar overall organisation [17]. These "secretins" are large oligomeric complexes with 3 or 4 rings of domains assembled parallel to the symmetry axis. Whether they share with Wza a helical transmembrane domain is unknown. However an analysis of the factors governing Wza assembly and in particular its helical transmembrane region may have significance for a wider range of bacterial outer membrane channels [17].

Mutagenesis of Wza is an appropriate method for examination of the function of specific domains. A problem with such studies for Wza is that the available assays for Wza function are indirect and are based on detection of exported capsular polysaccharide Reconstitition of *in vitro* transport is impossible at this time due to complexity of a system where the transport substrate is a polyisoprenoid-linked polymer whose synthesis and export are coupled[11] . Ideally, to complement mutagenesis studies, X-ray crystal structures for Wza containing various mutations and under different crystallisation conditions would be solved. However considerable resources would be required to undertake such a study, and limitations on crystallisation conditions may preclude the study of many interesting conditions: For example 3D crystals of Wza have so far only been observed at acidic pH [22] and require the presence of a detergent micelle. We have therefore employed cryo-electron microscopy for the structural analysis of the protein since it can be applied with a wide range of experimental conditions and does not require crystalline protein [23]. Initially, we have focussed on conditions that roughly reproduce those for Wza crystallization [5] (pH5, citrate buffer) as a check of the fidelity of the procedure. We have also carried out studies at pH8 in Tris buffer, conditions where crystallisation is not observed [22]

Results

Mutagenesis of the R4 domain of Wza

The helical barrel of the Wza oligomer represents a unique structural feature in bacterial outer membrane proteins. Examination of the primary sequences of Wza homologs in other bacteria identifies conserved features in this domain (Figure 1a). In each case, the C-terminal domain contains two conserved stretches followed by a region of 6 charged residues. To investigate the functional significance of these sequences, C-terminal truncations of the Wza R4 helical domain were constructed and their effects on the function and quaternary structure of the oligomer were assessed (Figure 1b,c). Removal of the last 4 amino acid residues (-RWPN-^{Cter}) in Wza$^{\Delta CT4}$ has no discernible effect on the properties of the protein, with little or no change in the stability of the octameric complex in the membrane. The stability of the Wza quaternary structure in SDS and in the milder anionic detergent PFO, allows assays of the effects of mutations in specific domains on oligomer assembly/stability using a standard PAGE protocol. Stability of quaternary structure in harsh detergents such as SDS has been observed in Wza [4, 11] and for other outer membrane proteins, including secretins [15, 16, 19, 21, 24].

There is no detectable effect on capsule assembly when polymer is identified in western imunoblots of lysates from cells expressing Wza$^{\Delta CT\ 4}$ (Figure 1b). The resulting cells gain sensitivity to bacteriophage K30 (data not shown) which uses the capsular polysaccharide as

an essential receptor and the cell surfaces are labelled by immunofluorescence using K30-specific antibodies as a probe (Figure 1e). The polymer seen in western immunoblots is therefore exported. Previously, it was shown that N-terminal acylation of the Wza lipoprotein is important for function [11]. Non-acylated protein allowed polymer synthesis to procede but the resulting polymer was retained in the periplasm. Thus, synthesis and export can be uncoupled in some constructs. The immunofluoresence results presented here confirm that $Wza^{\Delta CT4}$ is sufficient for both synthesis and export.

The last 3 amino acid residues of Wza are disordered in the X-ray structure [5] and, in closely related species the last 2 residues are often missing from the Wza homologs (see Figure 1). It is therefore not surprising that the 4 residue truncation mutant has almost no effect on the protein. In contrast, the removal of 18, 24 or 35 amino acid residues from the C-terminus of the protein was found to have severe effects on the function of the protein (Figure 1b,e). These truncations increasingly destabilise the octameric complex in the membrane (Figure 1c,d). Whilst weak residual capsule formation is apparent with the 18- and 24-residue truncations, the removal of the last 35 residues gives rise to a completely capsule-deficient bacterium, as determined by resistance to bacteriophage K30 and the absence of surface labelling in immunofluorescence (Figure 1e). The strong correlation between the presence of stable octamer in the membrane (Figure 1c,d) and Wza function in capsule assembly (Figure 1b,e) suggests that Wza oligomers are absolutely required for capsule formation, in agreement with the hypothesis that Wza octamers form a central hydrophilic passage through which the polysaccharide is translocated [5]. Interestingly, neither the deletion of some, nor the entire C-terminal helix had a major effect on the membrane-localisation of Wza (Figure 1c). Presumably the targeting of Wza to the outer membrane is conferred by other factors, most likely the N-terminal lipid acylation of the Wza lipoprotein [5].

Analysis of the surface area buried within the R4 domain by oligomerisation [5] predicts that there should be a significant free energy contribution of the R4 region to the overall stability of the octamer, in agreement with the mutagenesis studies. A free energy change (ΔG) of +18 kJ mol^{-1} for dissociation is predicted from the X-ray crystal structure using the Protein interfaces, surfaces and assemblies (PISA) service of the European Bioinformatics Institute (http://www.ebi.ac.uk/msd-srv/prot_int/pistart.html) [25]. Domains R1, and especially R3, are also predicted to contribute to the stability of the octamer with ΔG of dissociation equivalent to +9 and +180 kJ mol^{-1} respectively. Surprisingly, domain R2 is predicted by the same algorithm to be destabilising for the octameric complex, with a ΔG of dissociation of -14 kJ mol^{-1}.

Electron Microscopy

Figure 2a illustrates the overall structure and behaviour of purified single particles of octameric Wza, using high contrast uranyl acetate stain at pH~4 (particles appear white against a dark background). As reported previously [26], a range of particle orientations are observed, but the homogeneity of the preparation is sufficient for single particle analysis. Stain accumulation at the centre of the particles is consistent with the partitioning of uranyl acetate into the hydrophilic channel running through the Wza complex [5]. Although such conventional negative staining provides a high signal:noise ratio, it has drawbacks for structure determination that have been described many times [23, 27, 28].

In order to overcome these various problems, unstained specimens can be imaged, where the protein is maintained in a hydrated state in a thin layer of vitreous buffer at ~80K[23]. The main drawback in this method is that a lower contrast is obtained because of the weak scattering by the light atoms in the protein. Figure 2b shows an area of an electron micrograph of unstained Wza complexes in a DDM-containing citrate buffer at pH5 at ~80K

(particles appear dark against a lighter background). These conditions are close to those employed for the crystallisation of Wza and its high resolution structure determination by X-ray crystallography [5, 22]. Particles selected for analysis are indicated by the boxes. Larger clusters (arrows), where two or more Wza complexes overlap/co-localise, were not selected. Because of the necessity for detergent, small particles that are probably free DDM micelles of ~70kDa [29] are also just identifiable in the micrographs (arrowheads). Detergent micelles in various morphological states have been studied extensively by cryo-electron microscopy[30-35]. Three dimensional structures of Wza under different conditions were obtained by single particle alignment and averaging. The resolutions of the 3D structures were estimated by splitting each dataset into two and calculating the correlation between 3D structures generated from each half dataset as a function of resolution[36]. For the lower-contrast cryoEM data, we also generated 3D structures from two separate datasets (one collected on film, the other on CCD camera), and then compared the two independent structures as a check of the fidelity of the procedure (Supplementary Figure 1). Figure 2c shows the Fourier shell correlation (FSC) plots for the cryo-EM datasets, with strong correlation to $1/20Å^{-1}$. . Using an arbitrary cut-off of FSC=0.5, then conservative resolution limits around $1/16Å^{-1}$ are obtained. However using a more statistically relevant criterion (3σ crossing point) that compensates for the reduction in each dataset to half the original [36], then a limit of about $1/14Å^{-1}$ resolution would be estimated for the larger cryoEM dataset.

Wza structure at pH5

The cryo-EM structure of Wza in DDM-containing buffer at pH5 is displayed in Figure 3. This structure was generated from an *ab-initio* starting model rather than from the X-ray crystallography-derived structure [5]. Figure 3a shows a side view of the octameric complex using a surface threshold of ~2σ above the mean density level (yellow) that encloses a volume expected for 8 Wza molecules and a ~70kDa micelle of DDM molecules (~400 kDa total mass). Embedded within the 2σ surface is the high resolution Wza structure determined by X-ray crystallography [5] which is also displayed below (purple, ribbon representation). The hydrophobic helical barrel (ring R4) is at the top and the other 3 rings of hydrophilic domains are as indicated (R3-R1). The overall shape and size of the cryo-EM-derived structure of Wza is similar to the X-ray crystallography-derived structure, which can be fitted within the lower resolution 2σ envelope almost exactly. Only the tips of the domains of R4 at the top of the structure and R1 at the bottom protrude from the electron microscopy boundaries (arrows), whilst a loop from the N-terminal region sticks out at the side (red arrowhead). At these tips and loops, higher temperature factors are found in the X-ray crystal structure, suggesting more potential for flexibility in these regions of the protein (Figure 1b and later discussion).

The correspondence with the X-ray crystal structure is illustrated in greater detail in Figure 3b, using a second surface (blue) at a higher density threshold (3σ above the mean density) that allows the positions of the major domains to be identified within the molecular envelope (yellow). In the side view shown, four higher density rings can be discerned, as well as individual monomers within the octameric complex (indicated by the white dashed arrows). A twist to the high density regions in the map is of the same hand and pitch versus the symmetry axis as in the X-ray crystal structure (curved dashed arrows). The fitting of the X-ray crystal structure to the EM map shows that the high density regions (blue surface) correlate with the least flexible regions of the crystal structure, as illustrated in the temperature factor-colour-coded representation of a Wza monomer on the right of Figure 3b. Conversely, regions displaying the highest temperature factors are likely to lie outside the high density regions, and for a few residues, outside the lower density envelope (yellow surface, Figure 1a). Nevertheless, the overall fit between the X-ray and cryo-EM structure is

very good, with an average map value of 2.6σ above the mean density for all atoms in the X-ray structure, and with an average value of 3.4σ for atoms with temperature factors < 34 $Å^2$ (see Table I). Moreover the EM-derived map displays a pore at the upper surface that leads into a central cavity. This cavity is sealed at the bottom by a bridging platform that is slightly inset, giving a concave bottom surface. These features correspond almost exactly to those described for the crystal structure [5]. A ring of density at the top of the EM map that surrounds ring R4 in the fitted Wza structure is the only area where density in the EM map is not matched by atoms in the Wza structure. This additional density is likely to be due to the presence of a torus-shaped micelle composed of DDM molecules. Apart from a few tightly-bound detergent molecules, X-ray crystallography-derived electron density maps of membrane proteins are normally devoid of density for the detergent micelle because of its flexibility and the local molecular disorder of the detergent head groups and hydrocarbon chains. Density consistent with detergent micelles has, however, been observed at low resolution in many EM studies of various detergents[30-35], and in EM of 2D crystals of proteins[37] as well as in 3D crystals studied by neutron diffraction [38]. The properties of these torus-shaped micelles are consistent with molecular dynamics simulations of membrane proteins and detergent [39]. Figure 3c illustrates how such a micelle could be formed around the hydrophobic surface of R4 in Wza using extended DDM molecules for the fitting (blue stick representations). This preliminary exercise could be improved by e.g. a molecular dynamics approach, but nevertheless provides further evidence that the R4 region of Wza is the membrane-spanning component.

Subtle differences between the EM map and the crystal structure for Wza are noticeable, as revealed by the slices through the map shown in Figure 4. On the right are four panels representing sequential slices perpendicular to the C8 symmetry axis (corresponding to the locations of the four rings of domains R1-R4), and on the left is a central slice parallel to the symmetry axis. The overall shape and volume of the cavity is almost the same as that determined for the X-ray structure (~15000$Å^3$), except in the R2 region, where it is marginally wider (diameter 50Å) . The slice parallel to the symmetry axis (left, Figure 4), suggests that a better agreement between the EM map and the crystal structure would require a small outward movement of the R2 domain (as indicated by the red arrows). Such motions in Wza remain purely hypothetical, but it is interesting to note that the PISA calculations described above predict that R2 will have a much greater tendency to move apart. More flexibility in the R2 ring is also suggested by the lower overall density in this region of the map. For functional reasons, Wza must allow an extended polysaccharide chain to pass through into the central vestibule of Wza, it is possible that using EM we are seeing evidence of this flexibility. Small differences between crystal structures and EM maps are often observed for dynamic molecular machines [40-42], and may be akin to ‘breathing’ motions reflecting the innate flexibility of the proteins.

Wza structure at pH8

A second low resolution 3D structure of Wza was generated with the protein maintained at pH8. The conditions were chosen to match those employed for the previously published EM structure of Wza [10, 26], that employed an ammonium molybdate negative staining protocol. In these earlier studies, the helical barrel, R4, was not resolved. The results for the unstained protein at pH8 are shown in Figure 5 and summarised in Table I. A slightly better resolution was obtained for this structure, probably because of the larger dataset. Overall the pH8 structure appears less elongated and slightly wider in diameter. As expected on the basis of the earlier data [10, 26], the top half of the helical barrel structure forming R4 was absent, and moreover the associated density that was modelled as a band of detergent in the pH5 structure was missing. The average map value for the fitted R4 domain atoms was considerably reduced as a consequence (Table I). The pH-induced changes in the R4 region

also affect the pore that connects the central cavity to the outside of the complex. At pH8 it is closed off (Figure 5, slice through the structure), presumably by rearrangement of some of the residues in the R4 domains, whereas at pH5, a 10Å-diameter channel is present (Fig. 4). This suggests that the absence of density for the R4 helical barrel in the earlier negative-staining study was caused by alkaline pH, rather than by the presence of the heavy atom stain itself, and this conclusion is supported by a third low resolution structure obtained from uranyl acetate stained Wza particles (Figure 6, Table I). Here, the protein was fixed by the stain at low pH (pH~4), and despite the dehydration of the protein and high heavy atom concentration under these conditions, density for the helical barrel region was recognisable.

The differences between the structures obtained at pH5 and pH8 are further illustrated using a slice along the C8 symmetry axis of the complex shown in the right hand panel of Figure 5. As for the pH5 structure, the weaker density of the R2 ring is somewhat outwardly displaced compared to the crystal structure, moreover the R1 ring also appears to be further from the central axis of the complex, giving rise to a noticeable ~20Å diameter opening at the centre of this ring of domains. The diameter of the internal cavity is somewhat larger than expected for the crystal structure as a result of the outward displacement of density in the R1 and R2 regions, but because the pore at the top of the cavity has been closed off, the volume of the cavity at pH8 is slightly less than in the crystal structure[5].

The pH-induced structural change was also investigated using circular dichroism as well as with tryptophan fluorescence measurements of the purified Wza complex. Circular dichroism measurements of Wza between pH 5 - 9 showed only minor changes in the overall spectrum, consistent with a hypothesis that global unfolding of the protein does not occur (data not shown). If the R4 helical domain were to be completely transformed to random coil in the transition from pH5 to pH8, then the α-helix contribution to the CD spectrum would be calculated to drop by ~5%. Such a small change would be difficult to resolve from noise in the CD spectra. Tryptophan fluorescence measurements of Wza as a function of pH did, however, show measurable changes: Transition from pH5 to pH8 was found to give rise to a 20% decrease in fluorescence intensity and a 5nm red shift in the emission maximum, consistent with a move to a more polar environment for some of the tryptophan residues (data not shown). There are 5 tryptophan residues in Wza, with two located towards each end of the helix forming the barrel R4 (Figure 1a). In the crystal structure, the C-terminal tryptophan is disordered [5] and hence will probably be surrounded by polar water molecules in solution. However, the aromatic side chain of W350, located towards the periplasmic side of the membrane, emerges into a region that would be predicted to be hydrophobic. Hence W350 could be a sensor of the conformation of the helical barrel region which may explain the fluorescence changes described above.

Discussion

Earlier EM studies of Wza were carried out under conditions that were different to those subsequently used for the crystallisation of the protein [10, 22, 26, 45]. Whilst the overall structures of the protein determined by EM and X-ray crystallography were similar, there were unexplained differences in the helical domain, R4. As illustrated in Figure 6, the helical barrel was not evident in the structure of Wza obtained in the presence of 6% w/v ammonium molybdate, 1% w/v trehalose at pH7.5. It was assumed that the absence of this domain was a result of either the heavy atom staining conditions, or the pH. In the studies presented here, in the absence of stain we found that this domain was particularly sensitive to the pH of the solvent. At mild acidic pH, the correspondence between the EM structure and the crystal structure was very good, including the helical domain R4 whereas, at pH8, density for this domain was partially absent. In addition, a structure for Wza determined in the presence of an alternative heavy atom stain (uranyl acetate), but at pH~4, displayed a

cone-like feature consistent with the helical barrel (Figure 6). As expected, the uranyl acetate-stained structure, which was obtained at room temperature in the high vacuum of the microscope, showed some shrinkage compared to the other Wza structures. This effect of dehydration is well documented for conventional negatively-stained specimens [27]. In summary, the helical barrel forming the R4 domain in Wza is more sensitive to the pH of the solvent than the presence of heavy atom stain. A structural transition between pH8 and pH5 is also detected by tryptophan fluorescence measurements of the Wza complex.

Despite the pH-induced changes in the R4 domain, the R1, R2 and R3 domains in the low resolution cryo-EM structures show a good overall agreement with the X-ray crystal structure of Wza (Figures 3-5). Domain R3 shows a particularly tight agreement, perhaps reflecting the prediction of strong stabilisation of the oligomer by this domain (ΔG of dissociation of +180 kJ mol^{-1}). In contrast, domain R2 in the EM structures of Wza obtained at both pH5 and pH8 has weaker density, and displays a position that has bulged outwards versus the X-ray structure. These changes may be a reflection of the apparent destabilisation of the Wza oligomer by this domain (ΔG of dissociation of -14 kJ mol^{-1}).

Examination of the amino acid sequence of the R4 helical domain in Wza may provide clues to the pH sensitivity (Figure 1). Candidate residues in *E. coli* K30 Wza lie at the C-terminal tip of the helix (K375, R376) and about halfway into the predicted membrane span (H365, D366, E369)[5, 8]. The latter residues bulge into the hydrophilic pore and are positioned such that they can hydrogen bond to each other in a ring resulting in a constriction of the pore halfway through the putative membrane spanning region. Since K375 and R376 appear to be largely dispensible for function, as tested here by mutagenesis, then we would argue that H365, D366, E369 are more likely to be mediators of the pH effect on the R4 domain. Deprotonation of at least one of these residues at alkaline pH, and the concomitant loss of ionic interactions may be sufficient to destabilise the helical barrel in its non-native detergent-solubilised state. As theoretical calculations based on buried surface area in the R4 domain in the crystal structure suggest that the octameric barrel is energetically favoured over a monomeric or disordered state, then high pH-induced destabilisation of the barrel probably comes at an energy cost equivalent to the loss of at least one charge-charge interaction per monomer.

Do the pH-induced changes described here have implications for our understanding of Wza assembly *in-vivo*? Comparison of the *E. coli* K30 Wza sequence with other related bacterial proteins (Figure 1a) shows that H365, D366 and E369 are not absolutely conserved, although there are clear requirements for charged and hydrophilic residues at these inward-facing positions in the barrel constriction region. Rather than any pH-modulated effect, it seems more likely that the flexibility of the helical barrel that we observe will have a general significance for the maturation of the protein and its insertion into the outer membrane. Wza is likely to be stabilised in the membrane by a range of interactions with lipid alkyl chains and head groups, quite different to the constraints within a detergent micelle.

The R4 helical barrel clearly has an important role in the maturation of Wza *in-vivo*. Deletion of half the helical portion ($Wza^{\Delta CT18}$) which also removes the charged residues in the constriction region, gives rise to a significant loss of assembled Wza octamers in the *E. coli* outer membrane. In the absence of significant sequence homology between Wza and outer membrane proteins involved in other types of secretion [17], or comparable structural information, it is difficult to conclude whether a transmembrane helical domain is likely to be a common motif in such systems, and some evidence suggest that a C-terminal helical domain may not be widespread. Structure-function correlation studies of PulD, one of the best studied outer membrane secretins, were carried out by inserting a 24 amino acid cassette at various locations in the protein, and mutants were assayed for complementation

of a PulD^{-} strain, expression levels and oligomerisation (by exploiting the stability of the oligomer on SDS-PAGE)[24]. Insertional mutation in the C-terminal region of PulD reduced complementation efficiency to ~20% of controls, but had little effect on the expression levels of the protein, nor on the outcome of the oligomerisation assay [24]. This would argue, in fact, that the PulD transmembrane region is not located at the C-terminus. In contrast, insertion into the N-terminal region of PulD had a drastic effect on complementation and also oligomerisation. Similar studies of structure-function relationships in other outer membrane proteins will help to determine whether transmembrane helical domains, as described for Wza, could be applicable to a much wider range of these proteins.

Experimental Procedures

Mutagenesis of Wza

The C-terminal deletions of Wza were constructed by insertion of stop codons into the wild-type *wza* gene in plasmid pWQ126 [4] using a protocol based on the QuikChange Site-Directed Mutagenesis Kit (Stratagene, La Jolla, California).

Constructs were analyzed in the *wza*-null strain *E. coli* CWG281 (*wza*$_{K30}$::*aacC1*, *wza*$_{22min}$::*aadA*; Gm^{r}, Sp^{r}) [4]. Bacteria were grown at 37°C to mid-exponential phase in Luria-Bertani (LB) medium supplemented with ampicillin (100 μg ml^{-1}) and then gene expression was induced by the addition of L-arabinose to 0.006% w/v (final concentration) during a further 3 h of growth. The growth rates of bacteria overexpressing the various Wza constructs (following induction) are reduced compared to the untransformed host strain. The variations were not found to influence the data for Wza localization, stability and capsule assembly (not shown). Using the standardized 3 h induction period, all samples were prepared from cells in early stationary phase. Cells were collected by centrifugation and analyzed as described below.

Polyacrylamide Gel Electrophoresis (PAGE) and western blot analysis of K30 capsular polysaccharides and Wza proteins—Whole cell lysates were boiled in sodium dodecyl sulfate (SDS)-PAGE loading buffer (2% SDS, 10% glycerol, 33.5 mM DTT, 62.5 mM Tris, pH 6.8, bromophenol blue) and then treated with 0.5 mg ml^{-1} proteinase K overnight at 55°C to digest proteins [46]. Polysaccharides were separated on NuPAGE 4-12% Bis-Tris gels (Invitrogen Life Technologies Inc., Burlington, Ontario) using MOPS electrode buffer (50 mM tris base, 50 mM MOPS, 1 mM EDTA, 0.1% SDS), transferred to nitrocellulose membranes, and immunoblotted with anti-K30 polyclonal antibody (1:500) [47].

For PAGE and western blot analysis of Wza proteins, cell envelopes were prepared by sonication followed by ultracentrifugation at 100,000 x *g* for 1 h. For SDS-PAGE, envelopes were suspended in SDS-PAGE loading buffer and proteins were separated using Laemlli electrode buffer on 10% resolving gels that contained SDS. SeeBlue Plus2 Pre-stained Standard (Invitrogen Life Technologies Inc., Burlington, Ontario) was used as a protein mass marker. Proteins were transferred to PVDF membranes and immunoblotted with anti-Wza polyclonal antibody [4]. Proteins were also separated using perfluoro-octanoate (PFO) rather than SDS in order to visualize native protein complexes. For PFO-PAGE, cell envelopes were suspended in PFO-PAGE loading buffer (50 mM Tris-HCl, pH 7.5, 10% glycerol, 4% NaPFO) and separated using PFO-PAGE electrode buffer (25 mM Tris, 192 mM glycine, 0.5% (w/v) NaPFO) on 10% resolving gels that lacked SDS, essentially as described [48]. WaaJ, bovine serum albumin, alcohol dehydrogenase, β-amylase, and apoferritin proteins were run on the same gel for protein mass markers. Proteins were

transferred to nitrocellulose membranes and immunoblotted with anti-Wza polyclonal antibody [4].

Immunofluorescence microscopy—Cells were prepared via a protocol based on that of Reid and Whitfield [12]. All centrifugation steps were carried out at 5000 x *g* for 5 min. Cell pellets were washed twice with phosphate-buffered saline (PBS) and incubated for 5 min at room temperature on 12-well Printed Microscope Slides (Carlson Scientific, Inc, Peotone, IL) coated with poly-L-lysine. Cells were fixed in 4% (v/v) formaldehyde at 4°C overnight, warmed to 37°C, then washed three times in PBS and incubated in 50 mM NH_4Cl for 10 min at room temperature to quench free aldehydes. Slides were blocked in 3% (w/v) BSA dissolved in PBS for 30 min at room temperature and then incubated overnight at 4°C in anti-K30 polyclonal antibody (1:100) [47]. After warming to 37°C, cells were washed three times in PBS and incubated with rhodamine red-conjugated goat anti-rabbit antibodies (1:50) (Jackson Immunoresearch, West Grove, PA) for 1 h at room temperature in the dark. Coverslips were mounted using Vectashield mounting medium (Vector Laboratories, Inc, Burlington, Ontario) and immunofluorescence was examined using a Zeiss Axiovert 200 microscope.

Sample preparation—Purification of DDM-solubilised Wza was carried out as described in [5]. pH5 and pH8 buffers were as follows: 10mM sodium citrate, 50mM NaCl, 0.004% (w/v) dodecyl maltoside, pH5 or 10mM Tris-HCl, 50mM NaCl, 0.004% (w/v) dodecyl maltoside (DDM), pH8.

Cryoelectron microscopy and image analysis—Cryo-EM samples were prepared by adding 3 microlitres of protein at 0.6mg/ml to one side of a 400 mesh/in Quantifoil copper grid with 1.2-1.3 micron diameter holes in the carbon film. Both sides of the grid were briefly blotted dry with Whatman No. 1 filter paper in a humidity-controlled chamber using a Vitrobot (FEI) device, and the grid was then plunged into liquid ethane at <100K. The grid was transferred to a Gatan cryo-holder and inserted into a FEI Tecnai G2 200kV transmission electron microscope equipped with a field emission gun. Images were recorded on Kodak 4489 film under low electron dose conditions and developed for 8min in double strength Ilford developer or on a 4kx4k Gatan CCD camera. Digitisation of micrographs was carried out at 1200dpi using a UMAX 3000 digital scanner. Other details are as detailed in Table I. Particles were selected interactively using the BOXER function within the EMAN software suite, and then corrected for the contrast transfer function (CTF) using the CTFIT utility within the same package[43, 44]. Particles were then low- and high-pass filtered at $0.08Å^{-1}$ and $0.005Å^{-1}$ respectively, before an initial 3D model was created with the EMAN 'startcsym' algorithm. This selects two small subsets (~3% each) of the dataset containing the particles most closely matching the selected N-fold symmetry (i.e. 'top' views) and bilateral symmetry (i.e. side views). The two class averages (top and side views) are then back-projected assuming an orthogonal relationship, generating a noisy (unsymmetrised) 3D model. The resulting model can be inspected to judge to what extent the N-fold symmetry holds. For the pH5 and pH8 structures, there was a clear 8-fold symmetry in the maps, as well as a visibly asymmetric side-view. Iterative refinement of the structures was then carried out, using the preliminary model as a reference for classification and alignment of the whole dataset. The convergence of the refinement was judged by comparing the structure from the nth iteration with that from the (n-1)th iteration using Fourier shell correlation as a measure. When no further improvement of this parameter was possible, convergence was assumed to have occurred. In addition, a comparison between back-projections of the final 3D structure and their corresponding class averages (as well as a check of the raw particles composing those class averages) allowed a visual appraisal of the refinement (see Supplementary Figure 2). The resolution of the map emerging from the final

iteration was assessed by splitting the dataset into two and calculating 3D structures from each half dataset. The Fourier correlation was calculated between the two separate structures as a function of the resolution shell [36]. In order to test for potential mis-alignment (by 180°) of side-view projections, the Fourier shell correlation was calculated between each structure and a second version generated by a 180°-rotation around the normal to the C8 symmetry axis. In each case the correlation fell off much more steeply than the correlation calculated by splitting the dataset into two, implying that such alignment errors did not significantly affect the final structures.

A final filter of the amplitudes was applied that was based on the radially-averaged structure factor amplitudes of the Wza crystal structure [5]. Maps derived by electron microscopy were displayed with the CHIMERA software package[49]; and the same software was employed to automatically fit the Wza crystal structure to the maps and to calculate the average map values of Wza atoms after fitting.

Negative staining

Negatively-stained specimens were prepared by 20s incubation of Wza at 0.05mg/ml in 10mM Tris-HCl, 50mM NaCl, 0.004% (w/v) dodecyl maltoside (DDM), pH8 with glow-discharged continuous carbon film electron microscope grids. After blotting semi-dry with Whatman No.1 filter paper, the grids were briefly washed twice with deionised water and then incubated for 30s with a 4% w/v uranyl acetate solution, pH~4. Single particle selection, image processing and 3D reconstruction were as described above and in Table I.

Tryptophan fluorescence and circular dichroism measurements—Wza protein was resuspended in the pH8 buffer at 80μg/ml and the fluorescence emission and excitation spectra were recorded at room temperature in a 150μl volume quartz cuvette with a 1cm path length in a Cary Eclipse fluorimeter with 10nm excitation and 5nm emission slits. Spectra were also recorded after the addition of 0.5μl of a 0.6M citric acid solution, giving a final pH of 5. The reversibility of the pH-induced fluorescence changes was confirmed by further addition of 10 μl of 1.5M Tris-buffer, pH8.8, yielding a final pH of 8.5. To obtain CD spectra at different pH values (pH 4-9), the protein (1.1mg/ml) contained in 20 mM Tris-Cl pH8, 50 mM NaCl and 0.008% DDM was diluted to 0.1 mg/ml into buffers were the Tris component was exchanged for one of the following: 100 mM of either AcH/NaAc pH4, AcH/NaAc pH5, NaH2PO4/Na2HPO4 pH6, NaH2PO4/Na2HPO4 pH7, NaH2PO4/Na2HPO4 pH8 or 20 mM Tris-Cl pH9. CD spectra (180nm to 260nm) were then recorded at room temperature using a Jasco J-810 spectrometer. Secondary structure analysis was performed using algorithms implemented in the Dicroweb-Server at Birbeck College (UK) [50].

Database searches and sequence analysis—A search of proteins sharing strong homology to Wza in terms of their amino acid sequence was carried out using the BLAST [51] search program and subsequent alignment of a subset of sequences was carried out using CLUSTALW [52, 53].

Supplementary Material

Refer to Web version on PubMed Central for supplementary material.

Acknowledgments

J.H.N. is a Biotechnology and Biology Sciences Research Council (BBSRC) Career Development Fellow, and acknowledges funding from a Wellcome Trust programme grant. C.W. holds a Canada Research Chair and acknowledges funding from the Canadian Institutes of Health Research.

References

1. Roberts IS. Bacterial polysaccharides in sickness and in health. The 1995 Fleming Lecture. Microbiology. 1995; 141(Pt 9):2023–2031. [PubMed: 7496512]
2. Roberts IS. The biochemistry and genetics of capsular polysaccharide production in bacteria. Annu Rev Microbiol. 1996; 50:285–315. [PubMed: 8905082]
3. Whitfield C. Biosynthesis and assembly of capsular polysaccharides in Escherichia coli. Annu Rev Biochem. 2006; 75:39–68. [PubMed: 16756484]
4. Drummelsmith J, Whitfield C. Translocation of group 1 capsular polysaccharide to the surface of Escherichia coli requires a multimeric complex in the outer membrane. Embo J. 2000; 19:57–66. [PubMed: 10619844]
5. Dong C, Beis K, Nesper J, Brunkan-Lamontagne AL, Clarke BR, Whitfield C, Naismith JH. Wza the translocon for E. coli capsular polysaccharides defines a new class of membrane protein. Nature. 2006; 444:226–229. [PubMed: 17086202]
6. Wugeditsch T, Paiment A, Hocking J, Drummelsmith J, Forrester C, Whitfield C. Phosphorylation of Wzc, a tyrosine autokinase, is essential for assembly of group 1 capsular polysaccharides in Escherichia coli. J Biol Chem. 2001; 276:2361–2371. [PubMed: 11053445]
7. Paiment A, Hocking J, Whitfield C. Impact of phosphorylation of specific residues in the tyrosine autokinase, Wzc, on its activity in assembly of group 1 capsules in Escherichia coli. J Bacteriol. 2002; 184:6437–6447. [PubMed: 12426330]
8. Drummelsmith J, Whitfield C. Gene products required for surface expression of the capsular form of the group 1 K antigen in Escherichia coli (O9a:K30). Mol Microbiol. 1999; 31:1321–1332. [PubMed: 10200954]
9. Collins RF, Beis K, Clarke BR, Ford RC, Hulley M, Naismith JH, Whitfield C. Periplasmic protein-protein contacts in the inner membrane protein Wzc form a tetrameric complex required for the assembly of Escherichia coli group 1 capsules. J Biol Chem. 2006; 281:2144–2150. [PubMed: 16172129]
10. Collins RF, Beis K, Dong C, Botting CH, McDonnell C, Ford RC, Clarke BR, Whitfield C, Naismith JH. The 3D structure of a periplasm-spanning platform required for assembly of group 1 capsular polysaccharides in Escherichia coli. Proc Natl Acad Sci U S A. 2007; 104:2390–2395. [PubMed: 17283336]
11. Nesper J, Hill CM, Paiment A, Harauz G, Beis K, Naismith JH, Whitfield C. Translocation of group 1 capsular polysaccharide in Escherichia coli serotype K30. Structural and functional analysis of the outer membrane lipoprotein Wza. J Biol Chem. 2003; 278:49763–49772. [PubMed: 14522970]
12. Reid AN, Whitfield C. functional analysis of conserved gene products involved in assembly of Escherichia coli capsules and exopolysaccharides: evidence for molecular recognition between Wza and Wzc for colanic acid biosynthesis. J Bacteriol. 2005; 187:5470–5481. [PubMed: 16030241]
13. Raman P, Cherezov V, Caffrey M. The Membrane Protein Data Bank. Cell Mol Life Sci. 2006; 63:36–51. [PubMed: 16314922]
14. Koebnik R, Locher KP, Van Gelder P. Structure and function of bacterial outer membrane proteins: barrels in a nutshell. Mol Microbiol. 2000; 37:239–253. [PubMed: 10931321]
15. Schulz GE. The structure of bacterial outer membrane proteins. Biochim Biophys Acta. 2002; 1565:308–317. [PubMed: 12409203]
16. Stathopoulos C. Bacterial outer membrane proteins: topological analyses and biotechnological perspectives. Membr Cell Biol. 1999; 13:3–21. [PubMed: 10661467]
17. Collins RF, Derrick JP. Wza: a new structural paradigm for outer membrane secretory proteins? Trends Microbiol. 2007; 15:96–100. [PubMed: 17275308]
18. Collins RF, Frye SA, Kitmitto A, Ford RC, Tonjum T, Derrick JP. Structure of the Neisseria meningitidis outer membrane PilQ secretin complex at 12 A resolution. J Biol Chem. 2004; 279:39750–39756. [PubMed: 15254043]

19. Frye SA, Assalkhou R, Collins RF, Ford RC, Petersson C, Derrick JP, Tonjum T. Topology of the outer-membrane secretin PilQ from Neisseria meningitidis. Microbiology. 2006; 152:3751–3764. [PubMed: 17159226]
20. Nouwen N, Stahlberg H, Pugsley AP, Engel A. Domain structure of secretin PulD revealed by limited proteolysis and electron microscopy. Embo J. 2000; 19:2229–2236. [PubMed: 10811614]
21. Chami M, Guilvout I, Gregorini M, Remigy HW, Muller SA, Valerio M, Engel A, Pugsley AP, Bayan N. Structural insights into the secretin PulD and its trypsin-resistant core. J Biol Chem. 2005; 280:37732–37741. [PubMed: 16129681]
22. Beis, K. Biochemistry. St Andrews; St Andrews: 2005. PhD Thesis; p. 310
23. Henderson R. Realizing the potential of electron cryo-microscopy. Q Rev Biophys. 2004; 37:3–13. [PubMed: 17390603]
24. Guilvout I, Hardie KR, Sauvonnet N, Pugsley AP. Genetic dissection of the outer membrane secretin PulD: are there distinct domains for multimerization and secretion specificity? J Bacteriol. 1999; 181:7212–7220. [PubMed: 10572123]
25. Krissinel E, Henrick K. Inference of macromolecular assemblies from crystalline state. J Mol Biol. 2007; 372:774–797. [PubMed: 17681537]
26. Beis K, Collins RF, Ford RC, Kamis AB, Whitfield C, Naismith JH. Three-dimensional structure of Wza, the protein required for translocation of group 1 capsular polysaccharide across the outer membrane of Escherichia coli. J Biol Chem. 2004; 279:28227–28232. [PubMed: 15090537]
27. Bremer A, Henn C, Engel A, Baumeister W, Aebi U. Has negative staining still a place in biomacromolecular electron microscopy? Ultramicroscopy. 1992; 46:85–111. [PubMed: 1481278]
28. Harris JR. Negative staining of thinly spread biological particulates. Methods Mol Biol. 1999; 117:13–30. [PubMed: 10327397]
29. Strop P, Brunger AT. Refractive index-based determination of detergent concentration and its application to the study of membrane proteins. Protein Science. 2005; 14:2207–2211. [PubMed: 16046633]
30. Flood C, Dreiss CA, Croce V, Cosgrove T, Karlsson G. Wormlike micelles mediated by polyelectrolyte. Langmuir. 2005; 21:7646–7652. [PubMed: 16089365]
31. Kumar R, Kalur GC, Ziserman L, Danino D, Raghavan SR. Wormlike micelles of a C22-tailed zwitterionic betaine surfactant: from viscoelastic solutions to elastic gels. Langmuir. 2007; 23:12849–12856. [PubMed: 18004899]
32. Oda R, Bourdieu L, Schmutz M. Micelle to vesicle transition induced by cosurfactant: Rheological study and direct observations. Journal of Physical Chemistry B. 1997; 101:5913–5916.
33. Rossi S, Karlsson G, Ristori S, Martini G, Edwards K. Aggregate structures in a dilute aqueous dispersion of a fluorinated/hydrogenated surfactant system. A cryo-transmission electron microscopy study. Langmuir. 2001; 17:2340–2345.
34. Soga O, van Nostrum CF, Fens M, Rijcken CJ, Schiffelers RM, Storm G, Hennink WE. Thermosensitive and biodegradable polymeric micelles for paclitaxel delivery. J Control Release. 2005; 103:341–353. [PubMed: 15763618]
35. Vinson PK, Bellare JR, Davis HT, Miller WG, Scriven LE. Direct Imaging of Surfactant Micelles, Vesicles, Disks, and Ripple Phase Structures by Cryo-Transmission Electron-Microscopy. Journal of Colloid and Interface Science. 1991; 142:74–91.
36. van Heel M, Schatz M. Fourier shell correlation threshold criteria. J Struct Biol. 2005; 151:250–262. [PubMed: 16125414]
37. Auer M, Scarborough GA, Kuhlbrandt W. Three-dimensional map of the plasma membrane H+-ATPase in the open conformation. Nature. 1998; 392:840–843. [PubMed: 9572146]
38. Prince SM, Howard TD, Myles DA, Wilkinson C, Papiz MZ, Freer AA, Cogdell RJ, Isaacs NW. Detergent structure in crystals of the integral membrane light-harvesting complex LH2 from Rhodopseudomonas acidophila strain 10050. J Mol Biol. 2003; 326:307–315. [PubMed: 12547211]
39. Patargias G, Bond PJ, Deol SS, Sansom MS. Molecular dynamics simulations of GlpF in a micelle vs in a bilayer: conformational dynamics of a membrane protein as a function of environment. J Phys Chem B. 2005; 109:575–582. [PubMed: 16851049]

40. Ranson NA, Farr GW, Roseman AM, Gowen B, Fenton WA, Horwich AL, Saibil HR. ATP-bound states of GroEL captured by cryo-electron microscopy. Cell. 2001; 107:869–879. [PubMed: 11779463]
41. Ranson NA, Clare DK, Farr GW, Houldershaw D, Horwich AL, Saibil HR. Allosteric signaling of ATP hydrolysis in GroEL-GroES complexes. Nat Struct Mol Biol. 2006; 13:147–152. [PubMed: 16429154]
42. Elad N, Farr GW, Clare DK, Orlova EV, Horwich AL, Saibil HR. Topologies of a substrate protein bound to the chaperonin GroEL. Mol Cell. 2007; 26:415–426. [PubMed: 17499047]
43. Ludtke SJ, Baldwin PR, Chiu W. EMAN: semiautomated software for high-resolution single-particle reconstructions. J Struct Biol. 1999; 128:82–97. [PubMed: 10600563]
44. Tang G, Peng L, Baldwin PR, Mann DS, Jiang W, Rees I, Ludtke SJ. EMAN2: an extensible image processing suite for electron microscopy. J Struct Biol. 2007; 157:38–46. [PubMed: 16859925]
45. Beis K, Nesper J, Whitfield C, Naismith JH. Crystallization and preliminary X-ray diffraction analysis of Wza outer-membrane lipoprotein from Escherichia coli serotype O9a:K30. Acta Crystallogr D Biol Crystallogr. 2004; 60:558–560. [PubMed: 14993692]
46. Hitchcock PJ, Brown TM. Morphological heterogeneity among Salmonella lipopolysaccharide chemotypes in silver-stained polyacrylamide gels. J Bacteriol. 1983; 154:269–277. [PubMed: 6187729]
47. Dodgson C, Amor P, Whitfield C. Distribution of the rol gene encoding the regulator of lipopolysaccharide O-chain length in Escherichia coli and its influence on the expression of group I capsular K antigens. J Bacteriol. 1996; 178:1895–1902. [PubMed: 8606162]
48. Ramjeesingh M, Huan LJ, Garami E, Bear CE. Novel method for evaluation of the oligomeric structure of membrane proteins. Biochem J. 1999; 342(Pt 1):119–123. [PubMed: 10432308]
49. Goddard TD, Huang CC, Ferrin TE. Visualizing density maps with UCSF Chimera. J Struct Biol. 2007; 157:281–287. [PubMed: 16963278]
50. Whitmore L, Wallace BA. DICHROWEB, an online server for protein secondary structure analyses from circular dichroism spectroscopic data. Nucleic Acids Res. 2004; 32:W668–673. [PubMed: 15215473]
51. Altschul SF, Gish W, Miller W, Myers EW, Lipman DJ. Basic local alignment search tool. J Mol Biol. 1990; 215:403–410. [PubMed: 2231712]
52. Thompson JD, Higgins DG, Gibson TJ. CLUSTAL W: improving the sensitivity of progressive multiple sequence alignment through sequence weighting, position-specific gap penalties and weight matrix choice. Nucleic Acids Res. 1994; 22:4673–4680. [PubMed: 7984417]
53. Chenna R, Sugawara H, Koike T, Lopez R, Gibson TJ, Higgins DG, Thompson JD. Multiple sequence alignment with the Clustal series of programs. Nucleic Acids Res. 2003; 31:3497–3500. [PubMed: 12824352]

Europe PMC Funders Author Manuscripts

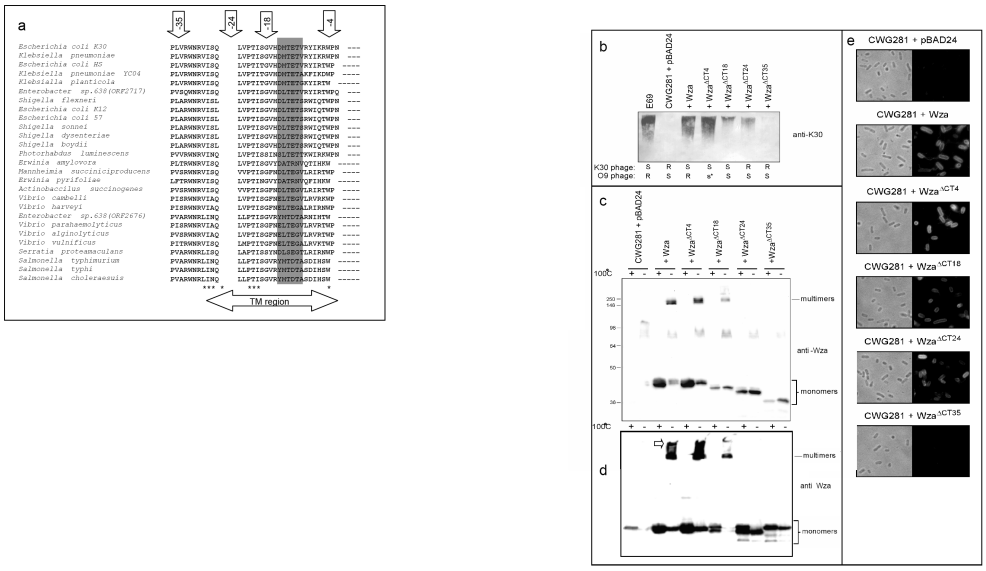

Figure 1.

Primary structure and function of Wza: (a) Comparison of the amino acid sequence of the *E.coli* K30 Wza C-terminal region (top row) with related proteins in other species, and strains with most closely related sequences at the top. The likely membrane spanning region (TM region) is indicated by the double-headed arrow at the bottom. The last 3 residues (WPN) are disordered in the crystal structure. The conserved residues (asterisks) tend to lie at the start of the long transmembrane helix {WNR-I} and {PTI} on the periplasmic side of the membrane. A region halfway through the membrane spanning region with charged residues that form a constriction of the inner pore, is indicated by the grey box (see discussion section). Wza-null CWG281cells transformed with the pBAD24 vector, or various Wza – containing plasmids were tested, as indicated and described in the main text. The C-termini of the four Wza truncation constructs that interfere with capsule biogenesis and with its ability to form stable multimers are indicated at the top (arrows). (b)) The synthesis of K30 polysaccharide was analyzed by anti-K30 immunoblots. Whole cell lysates from the parental strain E69 and transformed CWG281 were treated with proteinase K prior to electrophoresis. Truncation of the Wza C-terminal domain results in a loss of K30 polysaccharide. (c) SDS-PAGE and (d) PFO-PAGE of Wza-containing membranes after transfer to nitrocellulose and probing with anti-Wza polyclonal antibodies. When samples were not heated (-) prior to electrophoresis, multimeric Wza was detected as a high molecular mass band as indicated, but truncation of the C-terminal domain abolishes this behaviour. The migration of molecular mass marker proteins is shown on the left in (b), with the mass in kDa. The lower multimer band in the PFO-PAGE experiment migrated just above an apoferritin marker protein of 272 kDa. (e) Immunofluorescence microscopy with an anti-K30 antibody was used to assess the presence of K30 on the cell surface.

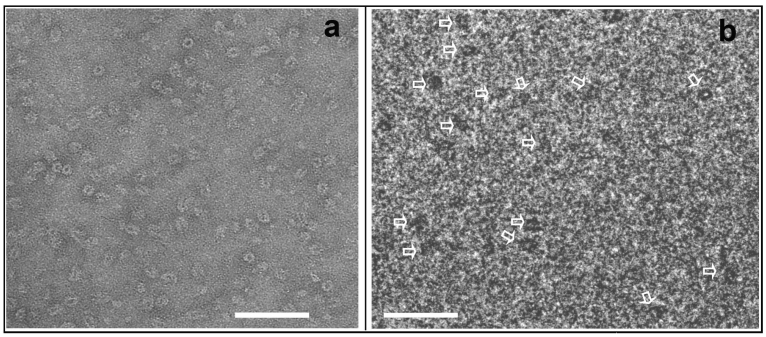

Figure 2.

Electron microscopy of Wza. (a) High contrast, uranyl acetate-stained Wza complexes at pH~4 (particles appear white against a dark background). A range of particle orientations are displayed, with side-on projections having roughly rectangular shape and bilateral symmetry, whilst face-on projections appear almost circular. Dark stain at the centre of the particles is consistent with the partitioning of uranyl ions into the hydrophilic channel running through the Wza complex, which is thought to provide the translocation pathway for capsular polysaccharide (ref). (b) Low contrast, unstained Wza complexes at pH5 embedded in vitreous water at ~80K (particles appear dark against a lighter background). Particles selected for analysis are indicated by the boxes. Some larger particles (arrows), probably aggregates of two or more Wza complexes, and small particles (arrowheads), probably free DDM micelles, were not selected. (c) Plot of the Fourier shell correlation (FSC) versus resolution for the 3D dataset obtained for unstained Wza complexes at ~80K and at pH5.

Europe PMC Funders Author Manuscripts

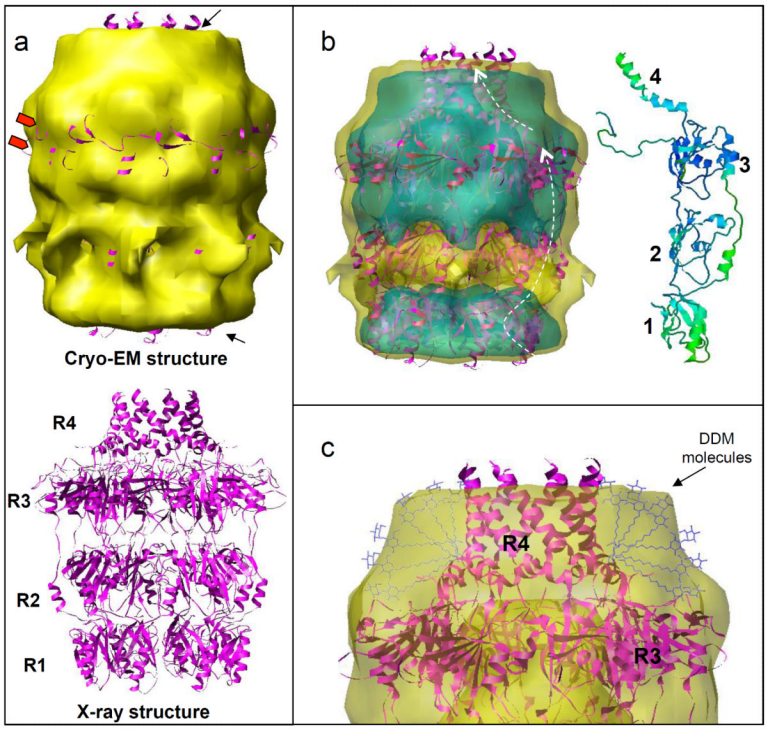

Figure 3.

Low resolution EM structure of the unstained octameric Wza complex in the presence of DDM and at pH5: (a) Top: surface-rendered view at 2σ above the mean density level (yellow). Bottom: ribbon representation of the high resolution Wza structure determined by X-ray crystallography (reference 5), with the hydrophobic helical barrel (ring R4) at the top with the other 3 rings of hydrophilic domains as indicated (R3-R1). (b) As in (a), but with partial transparency of the surface so that high density regions (4σ above the mean density) can also be discerned (blue surface). The fitted Wza structure is shown in purple, and to the right, a Wza monomer is shown, coloured according to temperature factors, with blue, green, yellow shades indicating increasing values (flexibility). The domains 1-4 are indicated. (c) The additional density in the EM map is roughly consistent with a band of DDM molecules (blue wireframe representation).

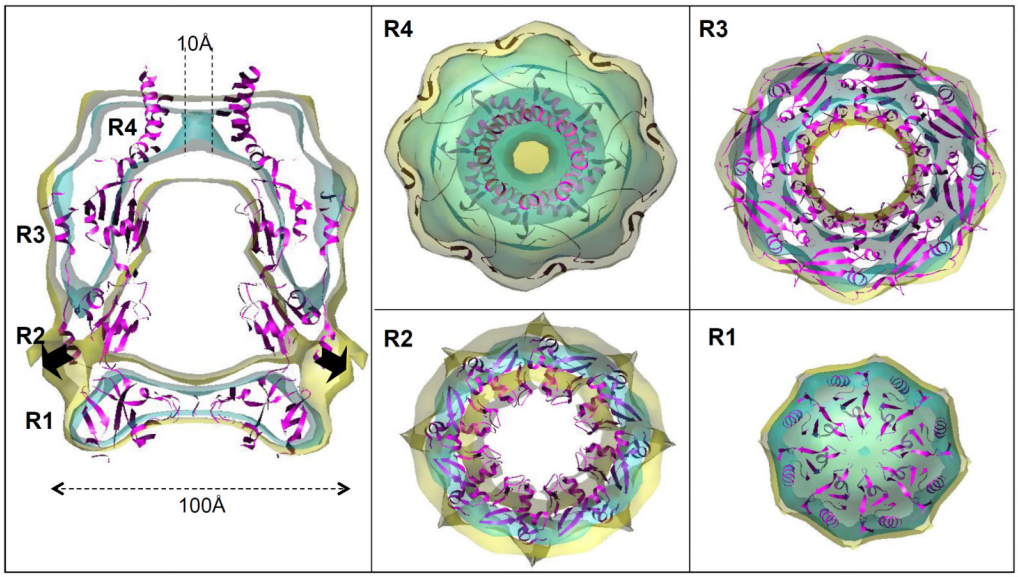

Figure 4.

Sections (slices) through the EM density map of Wza at pH5: The EM map is coloured as in Figure 3b, and the Wza X-ray crystal structure is shown in purple. On the right, four separate sections taken perpendicular to the C8 symmetry axis, representing the four rings of domains (R1-R4) are as indicated. For each section, the fit of the EM structure with the X-ray structure is good apart from the topmost (R4). Although this section displays the open central pore of the helical barrel, a ring of additional density on the periphery of the barrel is observed. On the left, a central section taken along the C8 symmetry axis is displayed. Conformational shifts required to bring domains in R2 and R1 into closer agreement with the EM structure are indicated by the white and red curved arrows (respectively). The central constriction of the R4 helical barrel region is indicated at the top, with a 10Å diameter aperture at the 4σ density level.

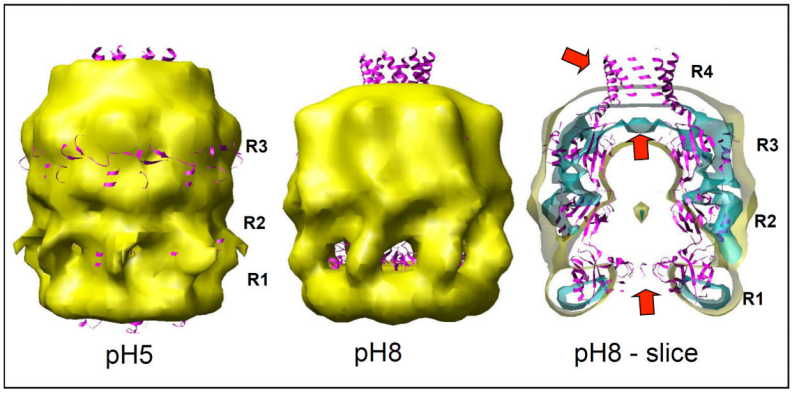

Figure 5.
Comparison of cryo-EM structures of Wza determined at pH5 (left) and pH8 (centre): A central slice through the pH8 structure is also displayed (right) with the fitted X-ray structure of Wza (purple ribbon trace). The blue and yellow surfaces for the pH8 map are at 2.9σ and 3.6σ above the mean density (see Table I). The three rings of domains R1-R3 are present in the pH8 structure, but the helical barrel R4 and the pore leading into the central hydrophilic cavity are altered compared to the pH5 cryoEM structure and the X-ray structure (red arrows).

Europe PMC Funders Author Manuscripts

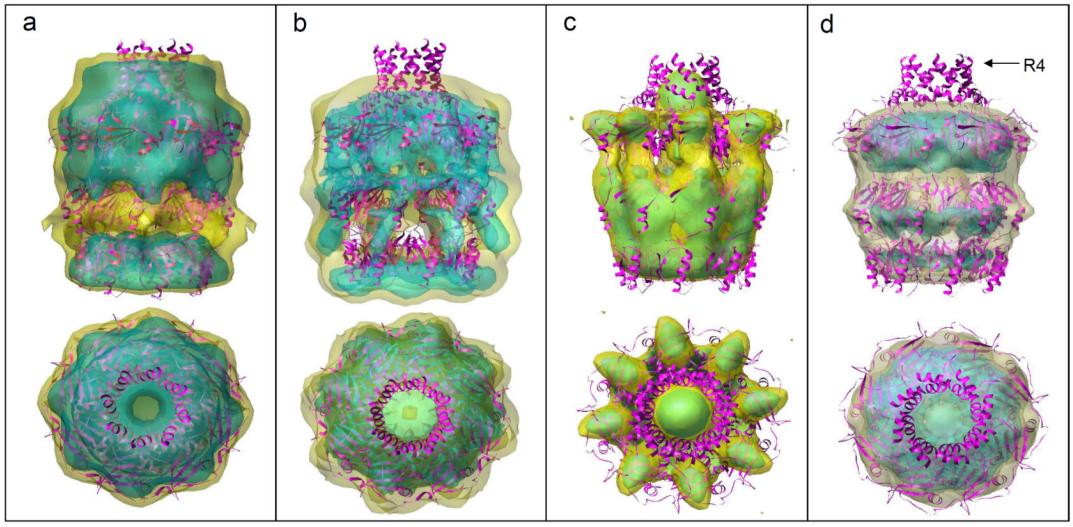

Figure 6.

Comparison of Wza structures: The high resolution structure determined by X-ray crystallography is represented by the purple ribbon trace in each panel. For the low resolution EM maps, high density regions are displayed within a lower density threshold which approximates the molecular envelope. (a) Wza at pH5, unstained, at ~80K. (b) Wza at pH8, unstained, at ~80K. (c) Wza in uranyl acetate at ~pH4 and 293K. (d) Previously reported Wza in ammonium molybdate/trehalose at pH7.5 and ~80K (reference 10). The structures for heavy-atom stained Wza (panels c & d) appear somewhat condensed compared to the unstained material (panels a&b). The configuration of the helical barrel domain (R4) at the top of the structure is strongly influenced by pH.

Europe PMC Funders Author Manuscripts

Table I

Parameters for the various Wza maps determined by electron microscopy and their correlation with the Wza X-ray crystal structure. For pH5 and pH8 maps, the information for the independent cryo-EM datasets collected on film or on CCD camera are displayed in standard font or in italics, respectively (if different).

	pH 5	pH 8	Negative Stain map (uranyl acetate)
Min, max, mean , rmsd (density).			−8.0 , +14.9, 0.0, 1.0
Resolution (FSC=0.5, 3σ crossover pt.).	15.5, 13.0	14.5, 12.7	25Å, 22Å
Symmetry applied.	C8	C8	C8
Angular increment used for 3D refinement.	6.0°	6.0°	9°
Map density threshold above the mean enclosing mass of 400kDa, 160 kDa.			1.5σ, 3.2σ
Defocus range used:	−1.4 to −5.3 μm *−1.7 to −5.3 μm*	−1.0 to −4.4 μm *−2.0 to −4.9 μm*	−0.2 to −0.8 μm
No. of particles selected. Total particles	4371 *4129* 8500	2468 *6838* 9306	3644
Scan step at the specimen level.	4.23Å *4.53 Å*	4.23Å *4.53 Å*	3.66Å
Primary magnification employed.	50000x *25000x*	50000x *25000x*	43700x
Average map value for fitted Wza crystal structure (21000 atoms)	2.6	2.7	1.8
Average map value for Wza atoms in R4 domain.	3.2	1.4	2.4